PROCEEDINGS OF SCIENCE

$K\pi$ scattering and excited meson spectroscopy using the stochastic LapH method

Ruairí Brett[*a], **John Bulava**[b], **Jacob Fallica**[c], **Andrew Hanlon**[d], **Ben Hörz**[e], **Colin Morningstar**[a]

[a] *Dept. of Physics, Carnegie Mellon University, Pittsburgh, PA 15213, USA*
[b] *Dept. of Mathematics and Computer Science and CP3-Origins, University of Southern Denmark, Campusvej 55, 5230 Odense M, Denmark*
[c] *Department of Physics and Astronomy, University of Kentucky, Lexington, KY 40506, USA*
[d] *Helmholtz-Institut Mainz, Johannes Gutenberg-Universität, 55099 Mainz, Germany*
[e] *PRISMA Cluster of Excellence and Institute for Nuclear Physics, Johannes Gutenberg-Universität, 55099 Mainz, Germany*
E-mail: rbrett@cmu.edu

Elastic $I = 1/2$, s- and p-wave $K\pi$ scattering amplitudes are simultaneously calculated using a Lüscher style analysis on a single ensemble of dynamical Wilson-clover fermions at $m_\pi \sim 230$ MeV. Partial wave mixing due to the reduced rotational symmetries of the finite volume is included up to $\ell = 2$. We also present finite-volume QCD spectra on two large anisotropic lattices ($32^3 \times 256$, $24^3 \times 128$) with $m_\pi \sim 230,\ 390$ MeV respectively. In each symmetry channel, a large basis of one- and two-hadron interpolating operators is employed with all-to-all quark propagation treated using the stochastic LapH method.

The 36th Annual International Symposium on Lattice Field Theory - LATTICE2018
22-28 July, 2018
Michigan State University, East Lansing, Michigan, USA.

*Speaker.

PoS(LATTICE2018)071

1. Introduction

As most excited hadrons appear as unstable resonances in experimental scattering cross sections, to study such states, first-principles determinations of hadron-hadron scattering amplitudes in QCD are desirable. Monte Carlo estimates in lattice QCD must be done in finite volume and using imaginary time, so directly determining scattering amplitudes is not possible. Using a particularly successful approach introduced by Lüscher, this difficulty can be circumvented by inferring infinite-volume scattering amplitudes from interacting finite-volume energies [1]. Further developed in Refs. [2, 3, 4, 5, 6, 7], among others, the method is now well established in the calculation of 2-to-2 scattering amplitudes. In this talk, a recent determination [8] of elastic $K\pi$ scattering amplitudes is presented, where the partial wave mixing due the the finite-volume is treated explicitly. Using the procedure outlined in Ref. [7], s- and p-wave amplitudes are determined, the latter being well-described by a Breit-Wigner form, as expected in the presence of a narrow $K^*(892)$ resonance.

Above three-particle thresholds, the formalism for extracting scattering observables is maturing (e.g., Refs. [9, 10]), with the first application to QCD appearing recently in Ref. [11]. As such, understanding the resonant spectrum in this regime from first principles calculations remains a challenge. The second half of this talk presents preliminary results from a qualitative determination of the excited spectrum of QCD in a set of $I = 1$ bosonic symmetry channels. By employing large bases of interpolating fields for single- and multi-hadron operators both the single-hadron dominated states and states with significant mixing with multi-hadron operators can be disentangled.

2. Finite-volume spectrum determination

In order to extract the finite-volume spectrum in a given symmetry channel, the $N \times N$ matrix $C_{ij}(t) \equiv \langle O_i(t+t_0)\overline{O}_j(t_0)\rangle$ of correlation functions is evaluated using the stochastic LapH method [12]. By solving the generalised eigenvalue problem (GEVP)

$$C(t_d)v(t_0,t_d) = \lambda(t_0,t_d)C(t_0)v(t_0,t_d), \tag{2.1}$$

for a single pair of diagonalisation times (t_0,t_d), the diagonal elements of the 'rotated' correlation matrix formed by the eigenvectors $v_n(t_0,t_d)$

$$\widetilde{C}_n(t) = (v_n, C(t)v_n), \tag{2.2}$$

can be fit with single or multi-exponential fits to extract the N lowest energies in the spectrum. The overlaps $Z_j^n = \langle 0|O_j|n\rangle$ between the initial set of operators and the finite-volume eigenstates can then be estimated. For the scattering amplitude analysis described in Sec. 3, as the signal of interest is the deviation of two-particle energies from their non-interacting counterparts, the so-called *ratio fits* of Ref. [13] are used.

3. Scattering amplitudes from finite-volume energies

Finite-volume energies are determined in the 'lab' frame in which the two-particle systems may have non-zero total momentum. In the centre-of-mass frame we define for $K\pi$ scattering the

following kinematic quantities

$$E_{\text{cm}} = \sqrt{E^2 - \mathbf{P}_{\text{tot}}^2}, \qquad \mathbf{q}_{\text{cm}}^2 = \frac{1}{4}E_{\text{cm}}^2 - \frac{1}{2}(m_\pi^2 + m_K^2) + \frac{(m_\pi^2 - m_K^2)^2}{4E_{\text{cm}}^2}, \tag{3.1}$$

where E is the lab frame energy determined above. The relationship between the two-particle centre-of-mass energies and the infinite-volume scattering amplitude can be expressed as [7]

$$\det[\widetilde{K}^{-1}(E_{\text{cm}}) - B^{(\Lambda,\mathbf{d})}(E_{\text{cm}})] = 0, \tag{3.2}$$

which holds up to exponentially suppressed corrections in the spatial extent L. $\widetilde{K}^{-1}$ and B are infinite-dimensional matrices in partial wave ℓ, and are real and symmetric, and Hermitian respectively, ensuring the determinant itself is real for real $\mathbf{q}_{\text{cm}}^2$. Expressions and software for numerical evaluation of the B-matrix elements are provided in Ref. [7]. For the scattering of spinless particles, following the convention of Ref. [8],

$$\widetilde{K}_\ell^{-1}(E_{\text{cm}}) \equiv \left(\frac{\mathbf{q}_{\text{cm}}}{m_\pi}\right)^{2\ell+1} K_\ell^{-1}(E_{\text{cm}}) = \left(\frac{\mathbf{q}_{\text{cm}}}{m_\pi}\right)^{2\ell+1} \cot\delta_\ell(E_{\text{cm}}), \tag{3.3}$$

is expected to be smooth near the elastic threshold. In the determinant condition in Eq. (3.2), partial wave mixing due to the reduced symmetry of the cubic finite-volume must be treated with care. In order to proceed with a practical computation, some truncation in ℓ is required. For a one-dimensional B, the determinant condition is, of course, trivial, yielding a one-to-one relationship between a finite-volume energy E_{cm} and an amplitude point $\widetilde{K}^{-1}(E_{\text{cm}})$. Here, however, as we consider $\ell \leq 2$, a parametrisation of each partial wave in $\widetilde{K}^{-1}$ is required with some number of fit parameters.

Irreps of the appropriate little group for various total momenta used in the $K\pi$ scattering analysis are listed in Table 1. While there are a number of irreps in which the $\ell = 1$ partial wave can be isolated, it is only the A_{1g} irrep at zero total momentum where $\ell = 0$ amplitude points can be unambiguously obtained. Hence, we determine both amplitudes simultaneously in the elastic region using the *determinant residual* method of Ref. [7].

$\mathbf{d}$	Λ	ℓ
$(0,0,0)$	A_{1g}	$0, 4, \ldots$
	T_{1u}	$1, 3, \ldots$
$(0,0,n)$	A_1	$0, 1, 2, \ldots$
	E	$1, 2, 3, \ldots$

$\mathbf{d}$	Λ	ℓ
$(0,n,n)$	A_1	$0, 1, 2, \ldots$
	B_1	$1, 2, 3, \ldots$
	B_2	$1, 2, 3, \ldots$
(n,n,n)	A_1	$0, 1, 2, \ldots$
	E	$1, 2, 3, \ldots$

Table 1: Irreps Λ of the appropriate little group for various total momenta $\mathbf{P}_{\text{tot}} = (2\pi/L)\mathbf{d}$ (where $\mathbf{d}$ is a vector of integers) considered in this work. We consider $K\pi$ systems at rest as well as those with non-zero total on-axis, planar-diagonal, and cubic-diagonal momenta. These momentum classes are listed in the first column, where $n \in \mathbb{Z}$.

4. Results: $K\pi$ scattering amplitudes

Based on the expectation of a narrow $K^*(892)$ resonance, the p-wave amplitude is well parametrised by a relativistic Breit-Wigner. For the s-wave amplitude we employ a variety of fit forms including generic linear and quadratic functions of $E_{\rm cm}$, motivated by analyticity of $\widetilde{K}^{-1}(E_{\rm cm})$ at threshold in $E_{\rm cm}$ and $s = E_{\rm cm}^2$ respectively. Additionally, we consider the NLO effective range expansion and an s-wave relativistic Breit-Wigner to parametrise the amplitude. As a test of the validity of the truncation in ℓ, the $\widetilde{K}$- and B-matrices are also enlarged to include d-wave contributions that we parametrise with the leading-order effective range expansion. Explicit expressions are provided in Ref. [8]. Simultaneous fit results from a single anisotropic ensemble with $N_f = 2+1$ clover-improved Wilson fermions, $(32^3|230)$, with $m_\pi \sim 230$ MeV are listed in Table 2. It is apparent that the $K^*(892)$ resonance parameters are insensitive to s-wave parametrisation and the inclusion of d-wave mixing. The amplitudes from fit 2 are shown in Fig. 1, together with the Breit-Wigner s-wave amplitude from fit 5, illustrating that different parametrisations for the s-wave produce a similar energy dependence in the elastic region. In addition to the fits, points from irreps without $\ell = 0, 1$ partial wave mixing are shown and seen to be consistent with the fit ansätze.

In the energy range in which we have determined the s-wave amplitude, some hint of the $K_0^*(800)$ may be expected to appear. From the LO effective range expansion, $m_\pi a_0 < 0$ suggests a virtual bound state. However, as the ratio $1 - 2r_0/a_0$ must be positive in the presence of a (real or virtual) bound state, using the NLO effective range parameters from fit 3 gives $1 - 2r_0/a_0 = -8.9(2.4)$. At the $3-4\sigma$ level then, we do not see any near-threshold bound state.

A careful analytic continuation, presumably requiring a better energy resolution than we have here, is needed to establish the existence of a $K_0^*(800)$ resonance pole above threshold on the second (unphysical) Riemann sheet. Nevertheless, we can obtain qualitative information about a possible s-wave pole by finding the zeros of $\mathbf{q}_{\rm cm} \cot \delta_0 - i\mathbf{q}_{\rm cm}$. This is easily done using the NLO effective range parametrization of fit 3 and solving the resultant quadratic polynomial, yielding $m_R/m_\pi = 4.66(13) - 0.87(18)i$ which is consistent with the Breit-Wigner mass and width from fit 4, which gives $m_{K_0^*}/m_\pi = 4.59(11)$ and $g_{K_0^*K\pi} = 3.35(17)$. It is important to remember here that in addition to the $K_0^*(800)$, the s-wave amplitude may also be influenced by the $K_0^*(1430)$ resonance. Without a full analytic continuation we can only infer qualitative information about a possible s-wave resonance pole from the elastic $\ell = 0$ amplitude calculated here.

Fit	s-wave par.	m_{K^*}/m_π	$g_{K^*K\pi}$	$m_\pi a_0$	χ^2/d.o.f.
1	LIN	3.810(18)	5.30(19)	−0.349(25)	1.49
2	QUAD	3.810(18)	5.31(19)	−0.350(25)	1.47
3	ERE	3.809(17)	5.31(20)	−0.351(24)	1.47
4	BW	3.808(18)	5.33(20)	−0.353(25)	1.42
5	BW	3.810(17)	5.33(20)	−0.354(25)	1.50

Table 2: Results for the $K^*(892)$ resonance parameters and the s-wave scattering length $m_\pi a_0$ from all fits to the amplitudes. For each fit, the p-wave amplitude is described using a relativistic Breit-Wigner. Fit 5 includes d-wave contributions as discussed in the text.

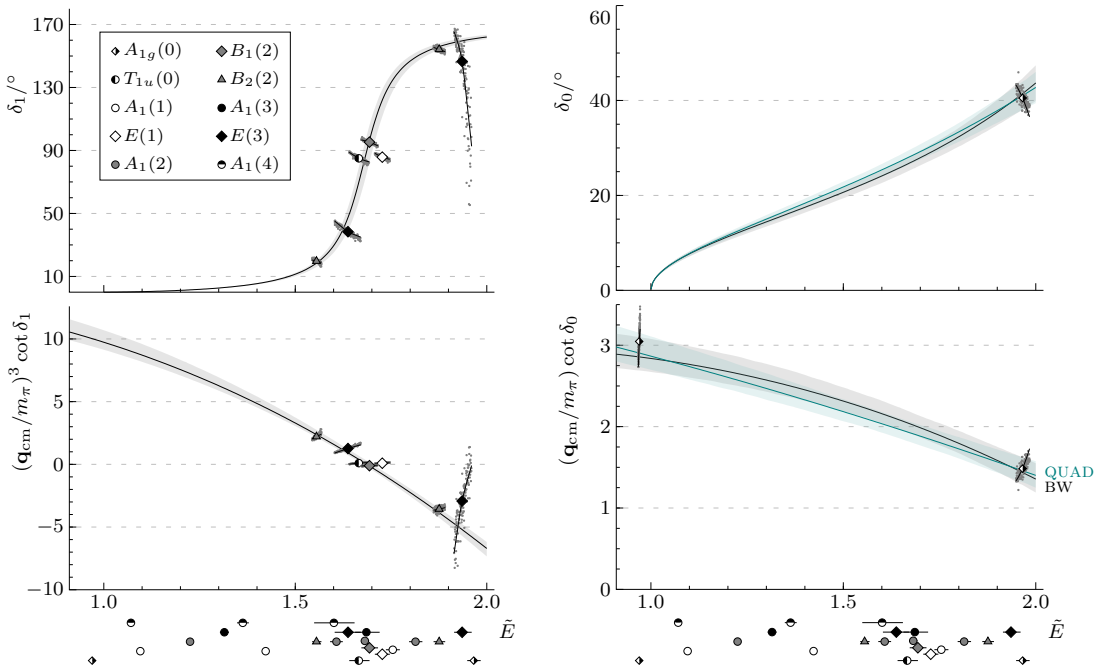

Figure 1: K-matrix fits to the s- and p-wave amplitudes as a function of $\tilde{E} = (E_{\rm cm} - m_K)/m_\pi$ such that the elastic region of interest extends over $1 < \tilde{E} < 2$. Together with the fits, which are explained in the text, we show amplitude points (neglecting d-wave contributions) from irreps with no mixing between s- and p-wave. All energies involved in the fit are indicated below the plots where they are offset vertically for clarity.

5. Results: excited meson spectroscopy

On two anisotropic ensembles $(32^3|230)$, $(24^3|390)$, with $m_\pi \sim 230, 390$ MeV respectively, we consider all isovector, non-strange, bosonic channels with negative parity and positive G-parity. In the interest of brevity, preliminary results are presented here for the resonance-rich T_{1u}^+ channel in which spin-1 and spin-3 states are expected to appear. In this symmetry channel we use a carefully selected set of 73 operators, 9 of which are so-called *optimised* single-hadron (SH) operators resultant from a preliminary GEVP using only SH operators chosen with care to best produce the expected spin-1 and spin-3 states in this channel. The remaining 64 two-hadron (MH) operators are chosen guided by the spectrum of all possible two-hadron states in the T_{1u}^+ symmetry channel assuming no interactions between the particles. Optimal interpolators for the expected hadronic states are chosen based on preliminary low-statistics runs and are described in detail in Ref. [14].

Using the Z overlaps for each operator onto the finite-volume energy levels, level identification can be performed based on the structure of the judiciously chosen probe operators. QCD being a complicated interacting quantum field theory makes this characterisation of stationary states difficult and largely qualitative. Nevertheless, we are well able to identify the stationary states expected to evolve into the single-meson resonances that correspond to quark-antiquark excitations in infinite-volume. For $m_\pi \sim 230$ MeV a staircase plot summarising the T_{1u}^+ finite-volume spectrum is shown in Fig. 2. In Fig. 3 we see that many more resonant states are seen in experiment than in our finite-volume calculation. There are multiple possible explanations for this, for example some states from experiment may not be simple quark-antiquark excitations but more exotic molecular states

that would not be clearly identified by our SH probe operators. More interesting however is the number of quark-antiquark identified stationary states found when considering only SH operators versus when mixing with MH operators is included. The appearance of an additional state in the energy range shown suggests that mixing between quark-antiquark excitations and two-hadron states is crucial for the reproduction of some states seen in experiment. Further investigation is required, with a finite-volume Hamiltonian based analysis for qualitatively describing the stationary state spectrum in progress. Note that we have not included any three- or four-particle interpolators despite going above the thresholds for creating such states.

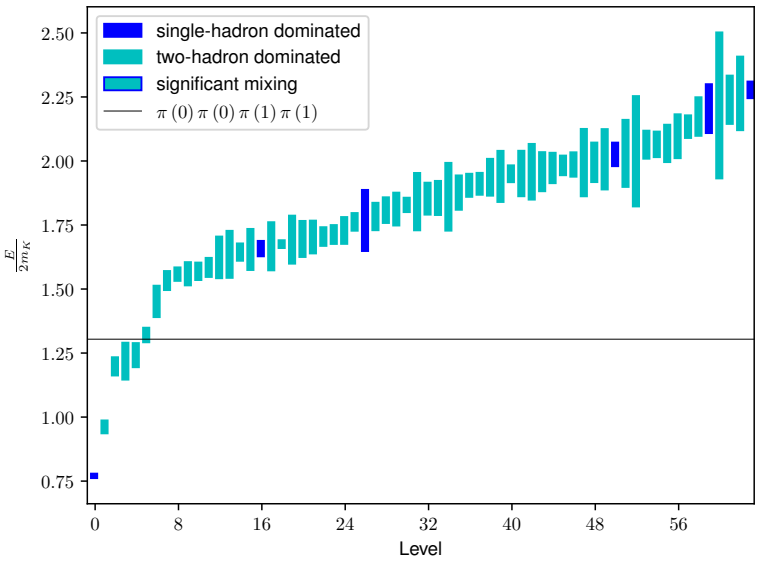

Figure 2: First 63 excited states in the isovector, non-strange T_{1u}^{+} channel with $m_\pi \sim 230$ MeV. Levels with maximal overlap onto the optimised single hadron (SH) and two-hadron operators (MH) are indicated by solid blue and cyan boxes respectively. Spectrum extracted using multi-exponential fits to diagonal elements of Eq. (2.2) from a GEVP with 73 operators (9 SH + 64 MH).

Acknowledgments

This work was supported by the U.S. National Science Foundation under award PHY-1613449. Computing resources were provided by the Extreme Science and Engineering Discovery Environment (XSEDE) under grant number TG-MCA07S017. XSEDE is supported by National Science Foundation grant number ACI-1548562.

References

[1] M. Lüscher, Nucl. Phys. B **354** (1991) 531.

[2] K. Rummukainen and S. A. Gottlieb, Nucl. Phys. B **450** (1995) 397.

[3] C. H. Kim, C. T. Sachrajda and S. R. Sharpe, Nucl. Phys. B **727** (2005) 218.

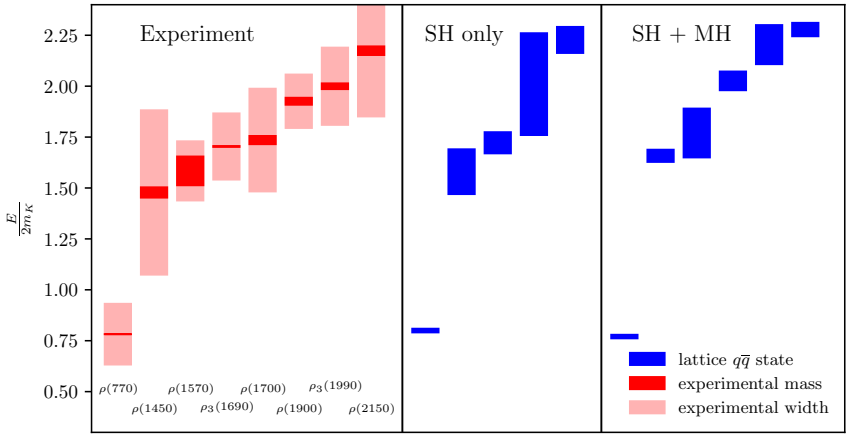

Figure 3: Comparison of experimental resonances (from Ref. [15]) to levels in the isovector, non-strange T_{1u}^{+} channel with $m_\pi \sim 230$ MeV which have dominant overlap with the single-hadron interpolators. The central plot contains the spectrum $\lesssim 5m_K$ as determined using only the single-hadron (SH) operators whereas the right column comes from the full spectrum determination using single- and multi-hadron (MH) operators. Note the emergence of an additional SH dominated level in this energy range with the inclusion of MH operators.

[4] M. Gockeler, R. Horsley, M. Lage, U. G. Meissner, P. E. L. Rakow, A. Rusetsky G. Schierholz and J. M. Zanotti, Phys. Rev. D **86** (2012) 094513.

[5] R. Briceño, Z. Davoudi and T. Luu, Phys. Rev. D **88** (2013) 034502.

[6] R. A. Briceño, Phys. Rev. D **89** (2014) 074507.

[7] C. Morningstar, J. Bulava, B. Singha, R. Brett, J. Fallica, A. Hanlon and B. Hörz, Nucl. Phys. B **924** (2017) 477.

[8] R. Brett, J. Bulava, J. Fallica, A. Hanlon, B. Hörz and C. Morningstar, Nucl. Phys. B **932** (2018) 29.

[9] R. A. Briceño, M. T. Hansen and S. R. Sharpe, Phys. Rev. D **95** (2017) 074510 .

[10] M. Döring, H. W. Hammer, M. Mai, J. Y. Pang, A. Rusetsky and J. Wu, Phys. Rev. D **97** (2018) 114508.

[11] M. Mai, and M. Döring, Phys. Rev. Lett. **122** (2019) 062503.

[12] C. Morningstar, J. Bulava, J. Foley, K. J. Juge, D. Lenkner, M. Peardon and C. H. Wong, Phys. Rev. D **83** (2011) 114505.

[13] J. Bulava, B. Fahy, B. Hörz, K. J. Juge, C. Morningstar and C. H. Wong, Nucl. Phys. B **910** (2016) 842.

[14] C. Morningstar, J. Bulava, B. Fahy, J. Foley, Y. C. Jhang, K. J. Juge, D. Lenkner and C. H. Wong, Phys. Rev. D **88** (2013) 014511.

[15] Particle Data Group collaboration, C. P. et al., Chin. Phys. C **40** (2016 and 2017 update).